JOURNAL OF MATERIALS SCIENCE 16 (1981) 1633–1642

The dependence of structure and conductivity in three-dimensional phosphate ionic conductors on composition

MASAYUKI NAGAI, SATORU FUJITSU, TAKAFUMI KANAZAWA
Department of Industrial Chemistry, Faculty of Technology, Tokyo Metropolitan University, Fukasawa, Setagaya-ku, Tokyo 158, Japan

HIROAKI YANAGIDA
Department of Industrial Chemistry, Faculty of Engineering, University of Tokyo, Hongo, Bunkyo-ku, Tokyo 113, Japan

Two series of solid solutions, $Na_xCa_{(1-x)/2}Zr_2(PO_4)_3$ (NCZP(x), $0 \leqslant x \leqslant 1$) and $Na_xNb_{1-x}Zr_{1+x}(PO_4)_3$(NNZP($x$), $0 \leqslant x \leqslant 1$), were synthesized. They were examined by powder X-ray diffraction, infra-red (i.r.) absorption and Raman scattering. Ionic conductivities of graphite coated samples were measured. A complete series of solid solutions was formed for NCZP(x), while a second phase was found for $x < 0.1$ for NNZP(x). The i.r. and Raman spectra of their solid solutions consistently showed the formation of PO_4 tetrahedra with different geometries. The composition dependence of conductivity is interpreted on the basis of a structural change around Na^+.

1. Introduction

The three-dimensional superionic conductor $Na_3Zr_2PSi_2O_{12}$ (NASICON) which is a solid solution in the system $NaZr_2(PO_4)_3$–$Na_4Zr_2(SiO_4)_3$, is considered to be possible candidate for the membrane of Na–S cells [1]. The crystal structure of both end members is rhombohedral ($R\bar{3}c$) and they have a large number of isostructural compounds such as $NaM_2^{IV}(PO_4)_3$ (M = Ge, Ti, Zr), $M^IM_2^{IV}(PO_4)_3$ (M^I = Li, Na, K, Rb, Cs, M^{IV} = Zr, Hf) and $Na_3M_2^{III}(PO_4)_3$ (M^{III} = Ti, Sc, Y, V, Cr) [2–6]. Therefore, these compounds are expected to form solid solutions. Investigation of the relationship between structure and conductivity in the series of solid solutions will give some information on factors affecting the conductivity. In this paper, the composition dependence of the conductivities for two different series of solid solutions, $Na_xCa_{(1-x)/2}Zr_2(PO_4)_3$ (NCZP(x), $0 \leqslant x \leqslant 1$) and $Na_xNb_{1-x}Zr_{1+x}(PO_4)_3$ (NNZP(x), $0 \leqslant x \leqslant 1$), are discussed on the basis of a structural change around Na^+ ions.

2. Experimental procedure

Mixtures of reagent-grade Na_2CO_3, $CaCO_3$, ZrO_2 and $NH_4H_2PO_4$ for NCZP(x), and Na_2CO_3, Nb_2O_5, ZrO_2 and $NH_4H_2PO_4$ for NNZP(x) were heated in platinum crucibles at 200° C and then at 900° C. The cake was powdered in an agate mill, the powder was formed into a disc by pressing isostatically at 98 MPa and then fired at 1300° C for 16 h. The products were examined by infra-red (i.r.) absorption (KBr method) and Raman scattering in addition to powder X-ray diffraction. For the Raman scattering experiments, the Ar emission line at 514.5 nm with an incident power of 100 mW was used. The lattice parameters were determined from least-square fit analysis. The diffraction intensities for the solid solutions with different compositions were calculated based on the parameters of $NaZr_2(PO_4)_3$. The fired samples were powdered again, formed into a disc and sintered at 1300° C for 16 h. A.c. conductivity measurements were carried out at 10 kHz using an LCR bridge for graphite coated samples. In order to minimize the influence of moisture, the data obtained on the cooling cycle were adopted. An electronic transport number was measured using a d.c. polarization method.

0022–2461/81/061633–10$03.00/0

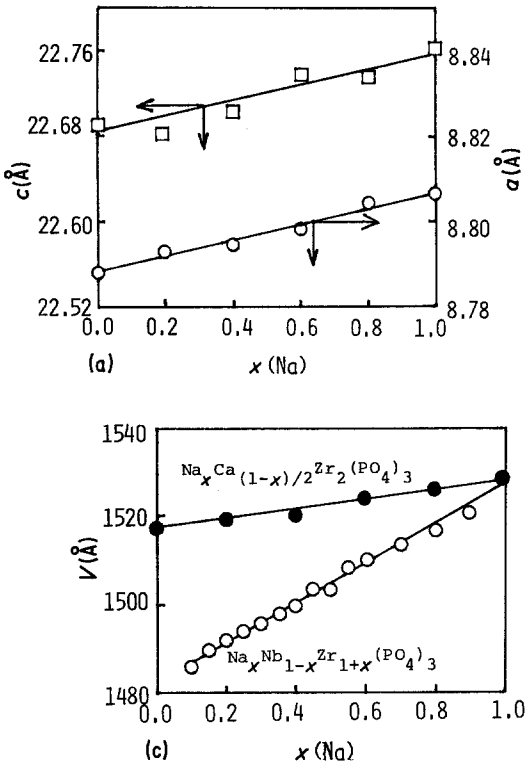

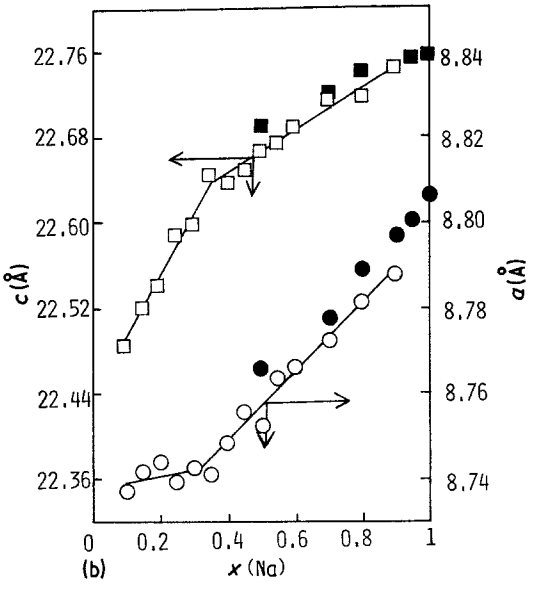

Figure 1 (a) Lattice parameters as a function of composition for NCZP(x) (hexagonal), ○: a, □: c, (b) lattice parameters as a function of composition for NNZP(x) (hexagonal), ○: a, □: c ●, ■; [8] and (c) cell volume against composition for NZCP(x) (●) and NNZP(x) (○).

3. Results and discussion

3.1. X-ray diffractions for NCZP(x) and NNZP(x)

A complete series of solid solutions was formed for NCZP(x), while a second phase was found below $x = 0.1$ for NNZP(x). Lattice parameters (hexagonal setting) of NCZP(x) as a function of composition are shown in Fig. 1a. Lattice parameters of the end member, $CaZr_4(PO_4)_6$, were almost the same as those of the previous work [7], while that of lattice parameter a differs slightly. The shrinkage rate along the a-axis was nearly equal to that along the c-axis (0.2 to 0.3% from $x = 0$ to 1). Fig. 1b shows the lattice parameters for NNZP(x) together with data obtained previously [8]. It is obvious that the data are divided into two regions. For $0.4 \leqslant x \leqslant 1$, both a and c shrink at the same rate (0.8 to 0.9% from $x = 0$ to 1); but the shrinkage of c is about ten times larger than that of a for $0.1 \leqslant x \leqslant 0.4$. If these parameters are plotted in a triclinic setting, the change is seen more clearly. The shrinkage along the c-axis is linear throughout the region whereas a is fixed for $0.4 \leqslant x \leqslant 1$, and increases with a decrease of Na content for $0.1 \leqslant x \leqslant 0.4$. Fig. 1c shows the unit cell volume (hexagonal setting) for both solid solutions, which indicates linear shrinkage for both series.

These results show that there is no large alteration in arrangement of atoms from the end member $NaZr_2(PO_4)_3$ except for NNZP($x = 0.1$ to 0.4). Consequently, it is useful to calculate the diffraction intensities for both solid solutions using the parameters for $NaZr_2(PO_4)_3$ as a primary standard [9]. The crystal structure is understood in terms of PO_4 tetrahedra and ZrO_6 octahedra which are linked at the corners forming a three-dimensional network, as illustrated in Fig. 2. Every oxygen atom simultaneously belongs to a PO_4 group and a ZrO_6 group. The sites of the sodium atoms are in the octahedra formed by the triangular faces of two ZrO_6 octahedra, as illustrated on the right-hand side in Fig. 2. The group $Zr_2(PO_4)_3^-$ is considered a major structural unit in the atomic arrangement. There are two crystallographically different sites for oxygen atoms, which are designated as O(1) and O(2). Each PO_4 tetrahedron is composed of two O(1) and two O(2) sites and Na^+ ions are located in Na_1 sites surrounded octahedrally by only O(2) atoms. In $NaZr_2(PO_4)_3$, there is a Na_2 site in addition to a Na_1 site, in the interstitial space which can accommodate extra Na^+.

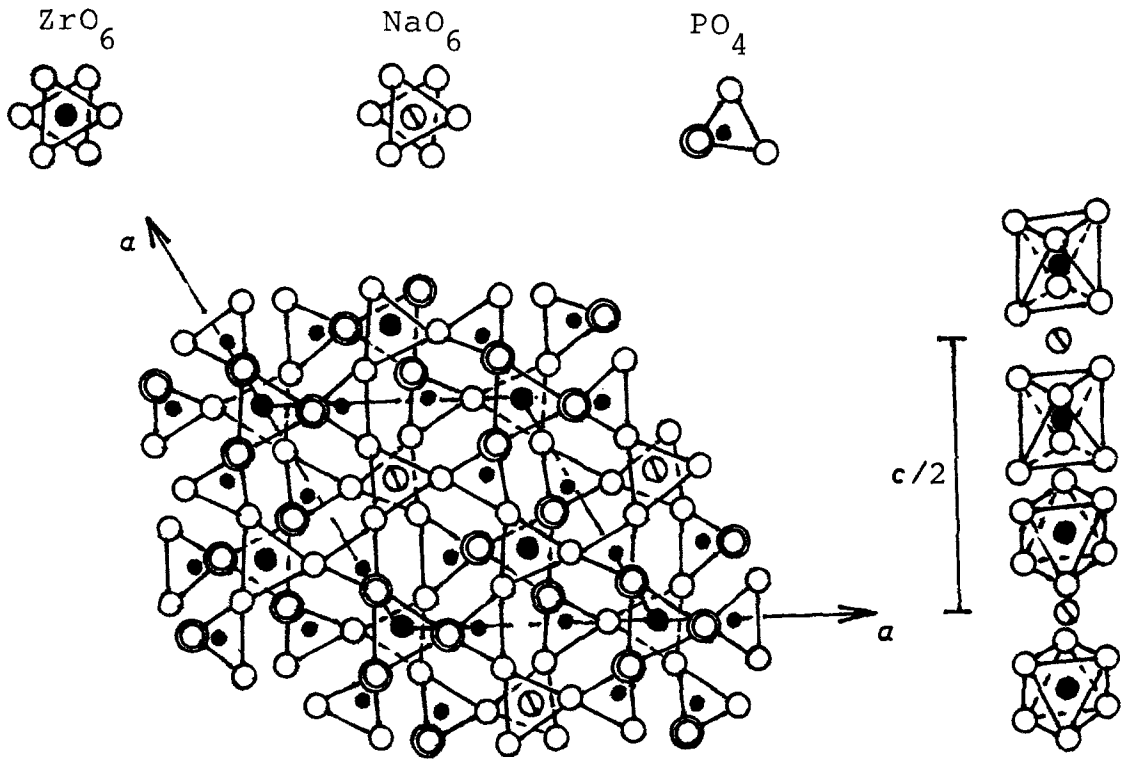

Figure 2 Schematic drawing for the crystal structure of $NaZr_2(PO_4)_3$.

The diffraction intensities (I) for $CaZr_4(PO_4)_6$ are calculated under the following conditions.

(1-a) Ca^{2+} substitutes Na^+ randomly and forms a Na^+ vacancy.

(1-b) The temperature factors do not change with replacement of Na^+.

(1-c) The arrangement of the other atoms are the same as in the previous state except for the isotropic shrinkage.

TABLE I Comparison of observed and calculated diffraction intensities for NCZP ($x = 1.0$)

Index	Intensity	
$h\,k\,l$	I_o	I_c
0 1 2	28	30
0 1 −4	79	83
1 1 0	93	100
1 1 3		
0 0 6	93	88
0 2 4	56	55
1 1 6		
1 2 −1	100	94
1 2 −4	23	27
0 3 0	39	41
R-factor	6.0	

The calculated intensities (I_c) are shown in Table I as well as the observed (I_o) ones. Comparison of I_c with I_o gave good agreement.

Similarly, the calculated intensities for NNZP(x) are obtained under the following conditions.

Similarly, the calculated intensities for NNZP (x) are obtained under the following conditions.

(1-d) Nb^{5+} substitutes Zr^{4+} randomly and a Na^+ vacancy forms in the neighbourhood.

(1-e) No change occurs in the temperature factors.

(1-f) The arrangement of the other atoms does not change.

The representative results for NNZP($x = 0.6$) are shown together with $NaZr_2(PO_4)_3$, NNZP($x = 1$), in Table II.

Since both end members for NCZP(x), $NaZr_2(PO_4)_3$ and $CaZr_4(PO_4)_6$, are isostructural and the ionic radius of Ca^{2+} (10.0 nm) is similar to that of Na^+ (10.2 nm), complete solid solutions are easily obtained. The significant difference in ionic radii between Nb^{5+} (6.4 nm) and Zr^{4+} (7.2 nm) will make it impossible to form the complete series of solid solutions for NNZP(x).

TABLE II Comparison of observed and calculated diffraction intensities for NNZP ($x = 1.0$) and NNZP ($x = 0.6$)

Index	NNZP ($x = 1.0$)		NNZP ($x = 0.6$)	
$h\,k\,l$	I_o	I_c	I_o	I_c
0 1 2	24	28	41	43
0 1-4	75	77	98	92
1 1 0	100	100	100	99
1 1 3	70	91	96	100
0 0 6				
0 2 4	45	49	63	60
1 1 6	80	79	97	80
1 2-1				
1 2-4	21	22	31	25
0 3 0	35	39	43	35
R-factor	8.0		8.8	

Additionally, the absence of Na^+ in the interstitial space which links $Zr_2(PO_4)_3^-$ frameworks will also increase the distortion. The replacement of Zr^{4+} by Nb^{5+} requires the relaxation of the neighbouring atoms. The large shrinkage along the c-axis for lower Na concentration may be attributed to this distortion.

3.2. Infra-red and Raman spectra for NCZP(x)

Fig. 3a shows infra-red (i.r.) spectra for NCZP(x) with different compositions. Four strong bands observed at 970, 1030, 1060 and 1200 cm^{-1} are specific to PO_4 tetrahedra. The band at 1200 cm^{-1} does not have a systematic tendency, but the others changed regularly. The bands at 970 and 1060 cm^{-1} both increased gradually with decreasing Na content, while that at 1030 cm^{-1} showed the opposite trend. Before assigning these bands, it is necessary to realize the geometry of PO_4 tetrahedra. According to the structural analysis [2], the P–O(1) bond length is about 15.2 nm and the P–O(2) bond length is about 15.5 nm. These values are less than the calculated single bond length of 17.1 nm [10], which indicates some double bond character. The partial double bond character of all bonds in PO_4 has been explained in terms of bonding between the empty 3d orbitals of phosphorus and the filled 2p orbitals of oxygen [11]. In $NaZr_2(PO_4)_3$, O(1) is only shared with a ZrO_6 octahedron, while O(2) is shared with a ZrO_6 and a NaO_6 octahedra simultaneously. If the electrostatic bond strength defined by Pauling [12] is calculated, assuming that all the M–O bonds in polyhedra are completely ionic and all the M–O bonds are equivalent, the results are as follows.

Since O(1) is surrounded by both a Zr^{4+}, which denotes a bond of strength 4/6, and P^{5+}, which denotes a bond of strength 5/4, the electrostatic bond strength for O(1) is 23/12. On the other hand, as O(2) is shared with a NaO_6 in addition to a ZrO_6 and a PO_4, that for O(2) is 25/12. The electron density of 2p orbitals of O(2) shifts more towards both Zr^{4+} and Na^+ than that of O(1) towards Zr^{4+}, thus reducing the participation of these obitals in bonding with the phosphorus atom. Consequently, the P–O(2) bond distance is larger than that of P–O(1). The difference is important because a PO_4 tetrahedron is surrounded by various kinds of cations or vacancies in these solid solutions. Similar facts were reported for i.r. and Raman spectra in $BaM^{IV}(XO_4)_3$ (M^{IV} = Ti, Ge, Zr, Hf; X = P, As) [13]. Concerning the influence of M–O bonding upon the stretching XO_4 vibrations, there was good correlation between these frequencies and the strength of the M–O bond. The possible geometries classified with respect to the nearest neighbour of the PO_4 tetrahedron are illustrated in Fig. 3c. The geometry 1-a is found in $NaZr_2(PO_4)_3$. If a small number of Na^+ are replaced randomly by Ca^{2+}, the geometries 1-b to 1-d are chiefly formed. These groups have C_s symmetry, whereas 1-a has C_{2v} symmetry. This lowering of symmetry may split the degenerate vibrations and activate i.r. inactive vibrations. Table III gives the number of i.r. and Raman active vibrations of the possible symmetries for PO_4 tetrahedral [14]. Therefore, the splitting shown in Fig. 3a may be explained by the lowering of symmetry from T_d to C_s. The Raman spectra shown in Fig. 3b indicate these splittings more clearly. There are at least 7 bands observed at 990, 1030, 1055, 1065, 1075, 1090 and 1220 cm^{-1}. The number of split bands cannot be interpreted only by the lowering of symmetry because the possible number of scattering bands ν_1 and ν_3 is, at most, 4. The bands at 1030, 1065 and 1090 cm^{-1} do not change in strength, while the remaining bands increase with decreasing Na concentration. These increased bands are thought to be caused by newly formed geometries. The PO_4 groups are classified on the basis of Pauling's electrostatic bond strength. If the average P–O bond strength, S_{P-O}, is defined by

$$S_{P-O} = 2 - \left(\frac{1}{4}\sum_i z_i/\lambda_i\right), \qquad (1)$$

where z is the formal charge of the cations, and λ

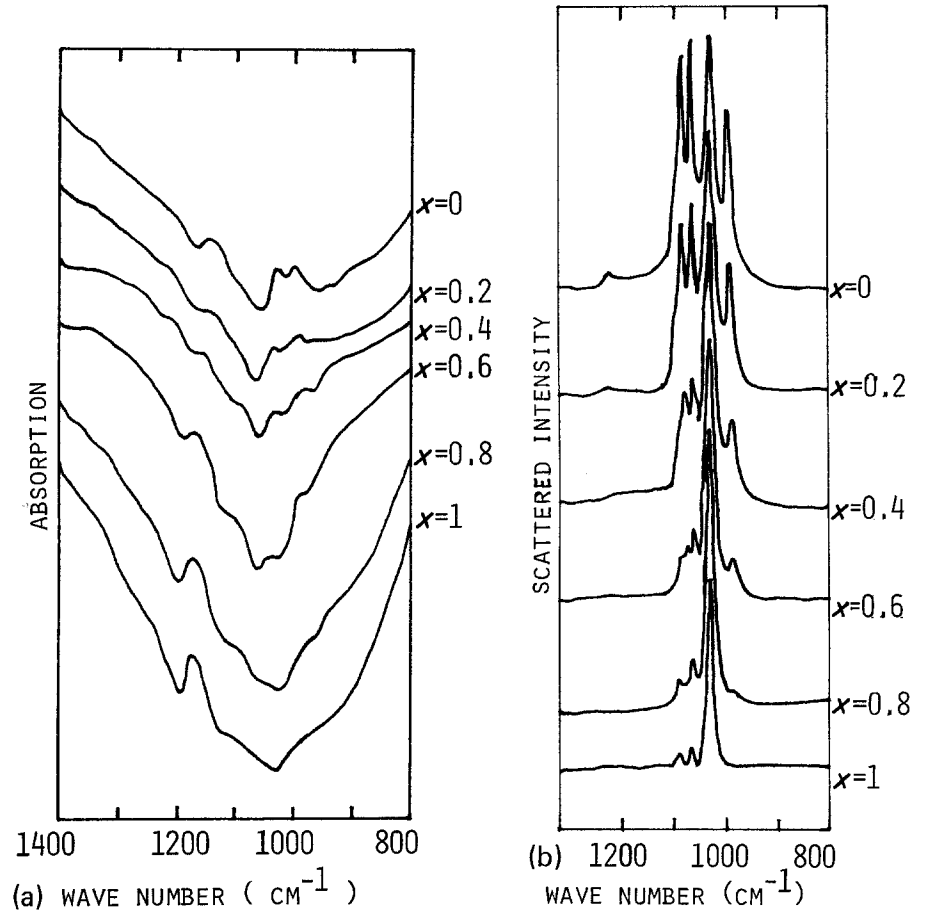

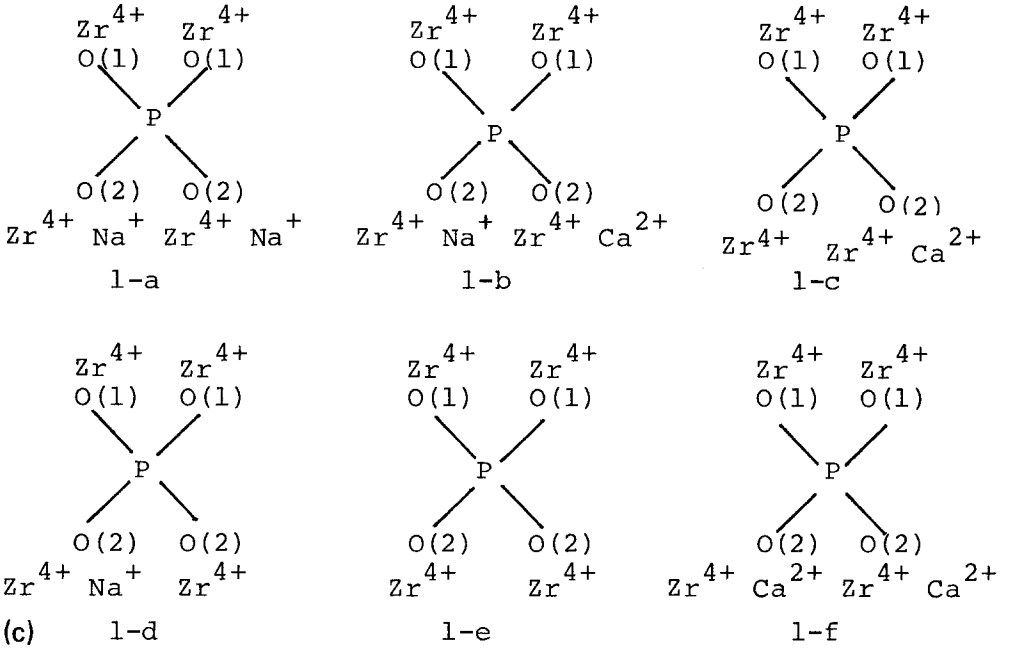

Figure 3 (a) Infra-red spectra for NCZP(x) with different compositions, (b) Raman spectra for NCZP(x) with different compositions and (c) geometries of PO_4 tetrahedra for NCZP(x).

TABLE III Numbers of infra-red and Raman active vibrations for the possible symmetries of PO_4 tetrahedra. IR: i.r. active, R: Raman active

Point group	Number of active vibrations			
	1	2	3	4
T_d	R	R	R, IR	R, IR
C_{3v}	R, IR	R, IR	2R, 2IR	2R, 2IR
C_{2v}	R, IR	2R, IR	3R, 3IR	3R, 3IR
C_s	R, IR	2R, 2IR	3R, 3IR	3R, 3IR

is the co-ordination number of the cations. The summation is obtained for all cations surrounding the PO_4 tetrahedron. The average P–O bond strengths are 1.25, 1.21, 1.25, 1.29, 1.33 and 1.17 for 1-a, 1-b, 1-c, 1-d, 1-e and 1-f, respectively. Since PO_4 groups from 1-a to 1-d are considered to exist mainly in the moderate Na content region, they will be classified as three types. $CaZr_4(PO_4)_6$ which includes the geometries 1-c, 1-e and 1-f, are also classified as three types. To obtain an idea of the change in P–O bond strength, the force constants are calculated by the GF matrix method, and bond orders and bond lengths are obtained following Robinon's empirical equations [15]

$$n_{P-O} = 0.119f + 0.74 \quad (2)$$

and

$$r_{P-O} = 17.6 - \left\{3.2 \Big/ \left[1 + 0.45\left(\frac{2-n}{n-1}\right)\right]\right\}, \quad (3)$$

where n is the bond order, f is a force constant and r is the bond length (nm). Interaction constants are neglected because of their slight contribution to the results. The parameters f, n and r are given in Table IV. They are obtained under the assumption that the symmetry is T_d and all the bands are assigned to ν_3 with different force constants except for the band at 1200 cm^{-1}. Comparing those bond lengths with the P–O bond of 0.152 and 0.155 nm in $NaZr_2(PO_4)_3$, they are slightly large but the change in length is a reasonable value. The results above consistently show that the split bands in the low Na content region may be explained by the formation of PO_4 tetrahedra with weak and strong bond strengths.

TABLE IV Comparison of force constants, bond orders and bond lengths for NCZP

Frequency (cm^{-1})	Force constant (f)	Bond order (n)	Bond length (r) (nm)
970	5.25	1.37	0.158
1030	5.92	1.44	0.156
1060	6.27	1.49	0.154

3.3. Infra-red and Raman spectra for NNZP(x)

Fig. 4a shows the infra-red spectra for NNZP(x) with different compositions. The main absorption bands which will be assigned to ν_1 and ν_3 are at 900, 1030, 1100 and 1200 cm^{-1}. The band at 1200 cm^{-1} shows no effect with decreasing Na^+ content. Both bands at 900 and 1100 cm^{-1} increase gradually, while the band at 1030 cm^{-1} decreases gradually. In contrast to NCZP(x), the number of possible geometries are large. For example, there are 18 different tetrahedra, even if the number of Nb^{5+} around the PO_4 group are limited to 2. The representative geometries which are thought to exist at high Na concentration are illustrated in Fig. 4c. The average bond strengths are 1.25, 1.21, 1.25, 1.29 and 1.21 for 2-a, 2-b, 2-c, 2-d and 2-e, respectively. Therefore, a similar classification to NCZP(x) is possible. The gradual increase at 900 and 1100 cm^{-1} indicates an increase in the number of PO_4 groups with strong and weak bond strengths. Although the band at 900 cm^{-1} can also be considered to be due to the vibrations of the NbO_6 unit, which is expected to dominate the 900 to 300 cm^{-1} region, the weak PO_4 group must be formed as well as the strong PO_4 group as 2-d to maintain electrical neutrality.

The parameters calculated by Equations 2 and 3 are given in Table V. All those values are reasonable except for the one at 900 cm^{-1}. This may be caused by the combination of at least two bands assigned to a PO_4 group and a NbO_6 group.

The bands of Raman spectra for NNZP(x) shown in Fig. 4b are very different from those for NCZP(x) (Fig. 3b). There are at least 8 bands at 925, 945, 1000, 1040, 1065, 1100, 1125 and 1215 cm^{-1} and those which appear in the low Na content region have a remarkably broad linewidth. The broad width and large number of bands will be due to the structural disorder around the PO_4 group, which suggests the formation of various kinds of geometry in addition to those in Fig. 4c.

3.4. Conductivity of NCZP(x)

Fig. 5 shows the composition dependence of σ_{150} (the conductivity at 150° C) and σ_N (the normalized conductivity) for NCZP(x). The σ_N is given

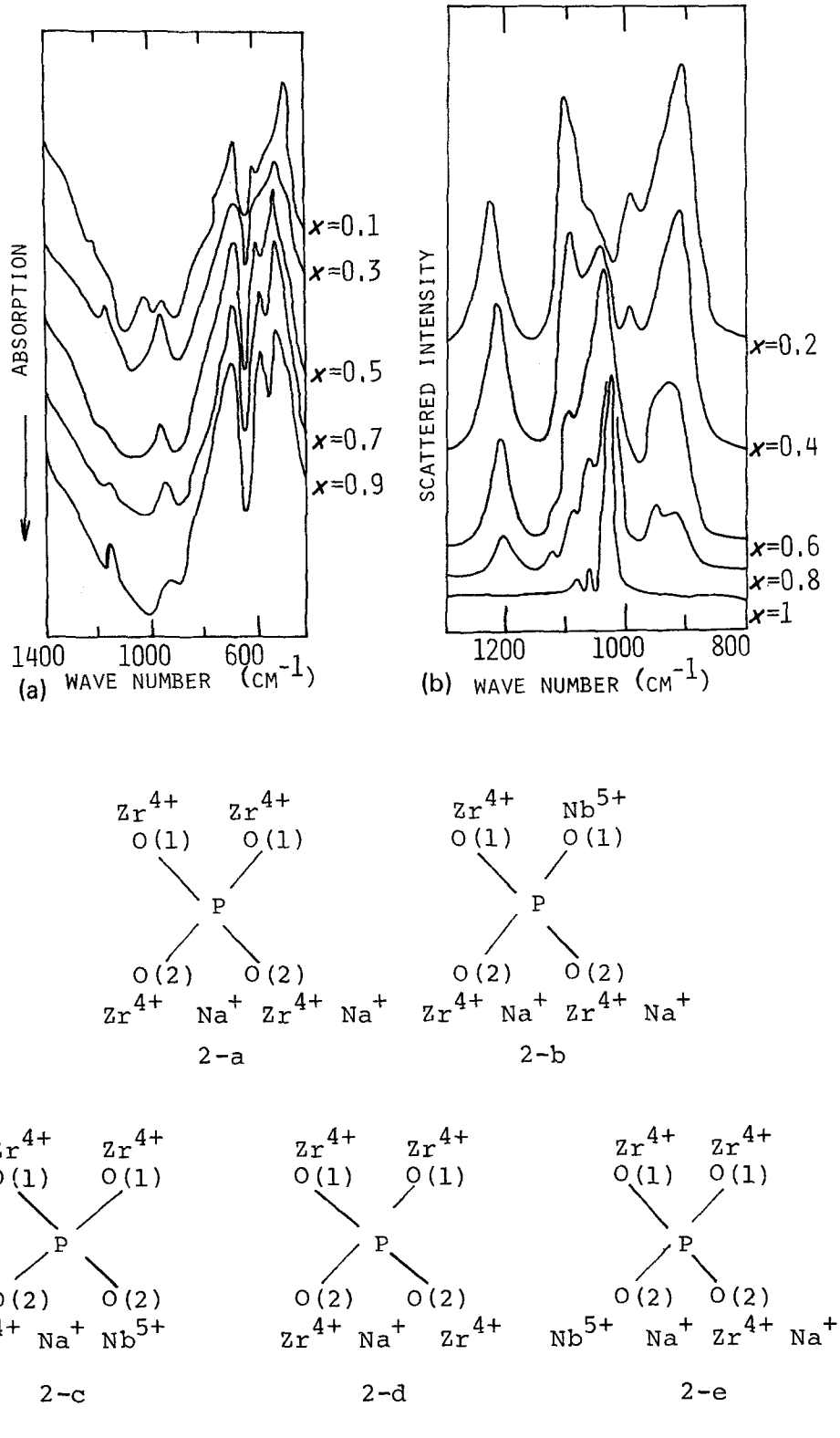

Figure 4 (a) Infra-red spectra for NNZP(x) with different compositions, (b) Raman spectra for NNZP(x) with different compositions and (c) representative geometries of PO_4 tetrahedra for NNZP(x).

TABLE V Comparison of force constants, bond orders and bond lengths for NNZP

Frequency (cm^{-1})	Force constant (f)	Bond order (n)	Bond length (r) (nm)
900	4.52	1.28	0.161
1030	5.92	1.44	0.156
1100	6.75	1.54	0.153

under the condition that the sample has the same carrier concentration, which roughly reflects Na^+ mobility because the electronic transport number for each sample is found to be negligible by the d.c. polarization method. The σ_{150} value decreases with decreasing Na concentration, whereas the σ_N is almost fixed. This result is in a striking contrast with β-Al_2O_3, which shows a remarkable decrease in σ on the replacement of a small quantity of Na^+ by Ca^{2+} [16]. The nuclear magnetic resonance spectrum (NMR) for β-Al_2O_3 suggests that the Ca^{2+} incorporated in the conduction plane hinders Na^+ motion [17]. As Ca^{2+} replaces Na^+ in the interstitial site, σ_N is expected to decrease considerably through the same effect as in β-Al_2O_3.

Generally speaking, the main factors affecting Na^+ mobility in a solid electrolyte with framework structures are considered as follows.

(1) Cross-sectional area in the interstitial space.

(2) Occupation ratios at the interstitial sites.

(3) Binding energy at the Na^+ site and/or the rigidity of the framework.

Co-operative motion, which is considered as one of the main factors in NASICON [19], is not important because Na^+ concentration is markedly small compared with the number of available sites. As described before, concerning the structure of $NaZr_2(PO_4)_3$, Na^+ exclusively occupies the Na_1 site, and the Na_2 site is left vacant. The first factor can be neglected because both the shrinkage of cell volume and the displacement of atoms are sufficiently small. About the second factor, the formation of a Na^+ vacancy at the Na_1 site increases the probability of Na^+ motion to the other site. Moreover, this factor is closely related to the third factor because substitution by other ions simultaneously changes the surroundings of Na^+. Therefore, it is essential to discuss the latter two factors together. The possible geometries in the Na region of moderate concentration are 1-a to 1-d in Fig. 3b. As the staying time at the Na_2 site is markedly short in comparison with that at the Na_1 site and the Na_1 site is surrounded only by O(2), Na^+ mobility will depend on the Na–O(2) bond strength. To avoid complexity it is assumed that the geometries 1-e and 1-f are not formed in this region. If 1-b is formed, 1-c and 1-d are formed in the neighbouring region. The Na–O(2) bond in 1-b becomes weaker than that in 1-a, because the substituted Ca^{2+} attracts the electron of 2p orbitals of O(2) and weaken the bonding between the empty 3d orbitals of P and 2p of O(2). Therefore, the remaining three P–O bonds become shorter, reducing the opposite Na–O(2) bond strength. This weakly bonded Na^+ can move more easily to the neighbouring site than the previous state. Consequently, the above increasing and decreasing factors cancel each other out and make the mobility independent of the composition of NCZP(x).

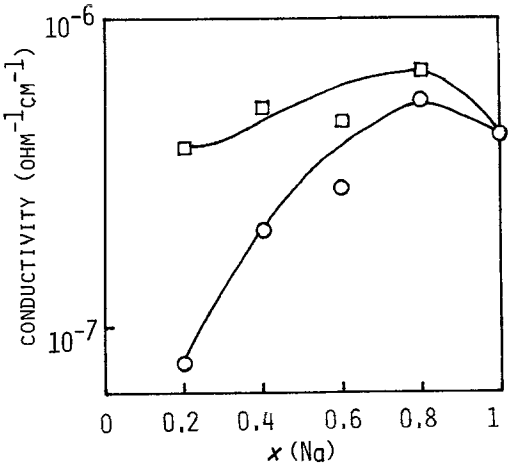

Figure 5 Composition dependence of σ_{150} and σ_N for NCZP(x), ○: σ_{150} □: σ_N.

3.5. Conductivity of NNZP(x)

Fig. 6a and 6b show the data for σ_{200} and σ_N, respectively. All these solid solutions with or without binders show maximum conductivity near $x = 0.4$ to 0.5, while σ_N indicates that Na^+ mobility has a maximum at lower Na^+ concentration than σ_{200} does. The solid solutions have the relative densities: 60 to 66% for no binders, 67 to 80% for $NaPO_3$ and 79 to 89% for SiO_2. Although the sample with the higher density shows higher conductivity, the general tendency in the composition dependence of conductivity for each solid solution is not changed even if the conductivity is corrected by considering the relative density. The electronic transport number was found to be negligible. With regard to the first factor, it has

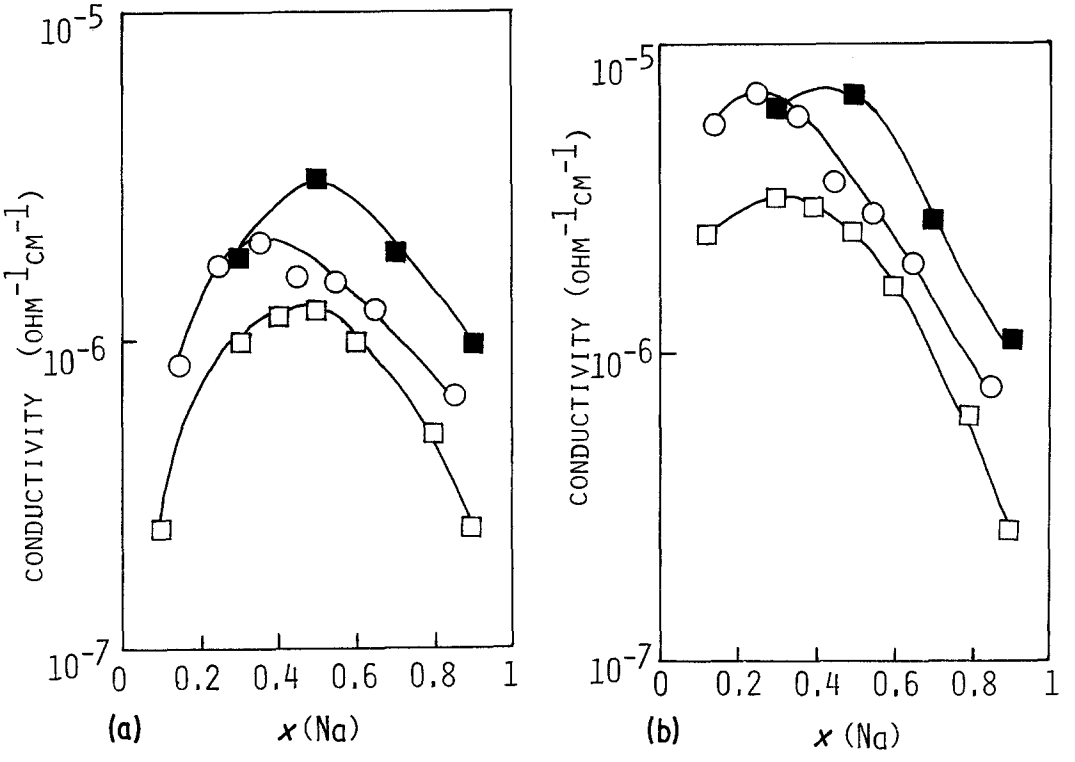

Figure 6 (a) Compositions dependences of σ_{200} for NNZP(x) with and without binders, □: no addition ○: $NaPO_3$ ■: SiO_2 and (b) composition dependences of σ_N for NNZP(x) with and without binders, □: no addition ○: $NaPO_3$ ■: SiO_2.

been reported that the conductivity of NASICON is more sensitive to the applied pressure than that of β-Al_2O_3 [18]. Therefore, the cross-sectional area of NASICON was though to be barely large enough to permit easy Na^+ movement. The cross-sectional area of the present solid solutions is less than that of NASICON. Consequently, the increase of σ_{200} in spite of the shrinkage in cell volume indicates the priority of the other factors. One possible explanation which is associated with the second and third factors is as follows. When Zr^{4+} is substituted by isolated Nb^{5+}, three b-type bonds and three c-type bonds are formed around Nb^{5+}, and three c-type bonds and three d-type bonds are formed around the Na^+ vacancy, where the notation corresponds to that in Fig. 4b. To realize the location of Na^+, a schematic drawing for Na^+ sites is illustrated in Fig. 7, where x, y_i and z_i denote the Na^+ vacancy and the nearest neighbour sites, respectively. The formation of a Na^+ vacancy at x will increase the probability of Na^+ movement from y_i or z_i to x_i. Additionally, substitution changes the third factor. The Na^+ at z_i is surrounded by five a-type bonds and one b-type bond which forms a weakly Na–O(2) bond owing to the reason described in Section 3.2. This weakly bonded Na^+ will also contribute to an increase in the probability of moving to the neighbouring vacant site.

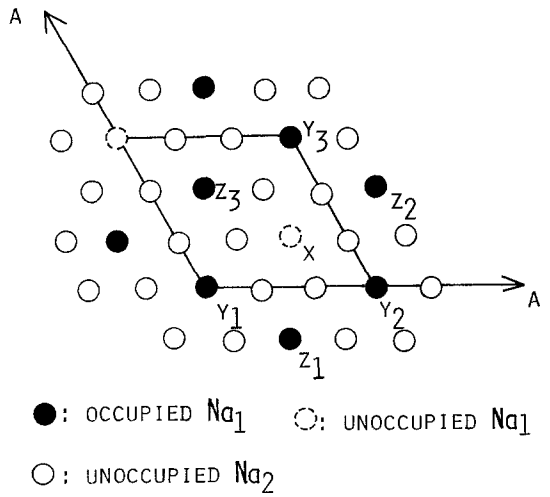

Figure 7 Schematic drawing for Na site.

In the moderate Na concentration region, Na^+ vacancies are distributed so closely that Na^+ can move a relatively large distance by this mechanism.

Although there are many more geometries in this solid solution system, which are suggested by Raman spectra, the increase in mobility in the lower Na content region supports the above idea.

4. Summary

The composition dependences of structure and conductivity for two different zirconium phosphates were examined.

4.1. $Na_xCa_{(1-x)/2}Zr_2(PO_4)_3$ (NCZP(x), $0 \leqslant x \leqslant 1$)

(1) A complete series of solid solutions with randomly distributed Ca^{2+} was formed.

(2) I.r. and Raman spectra are interpreted by the formation of PO_4 tetrahedra with different P–O bond strengths.

(3) The composition dependence of conductivity is accounted for by both the hindrance of Na^+ motion by Ca^{2+} and the change in the surroundings of Na^+.

4.2. $Na_xNb_{1-x}Zr_{1+x}(PO_4)_3$ (NNZP(x), $0 \leqslant x \leqslant 1$)

(1) Solid solutions with randomly distributed Nb^{5+} were formed except for compositions below $x = 0.1$.

(2) Anisotropic shrinkage of lattice constants was found for compositions below $x = 0.4$.

(3) I.r. spectra are interpreted in a similar way to NCZP(x), while the remarkable line broadening of Raman bands suggests structural disordering around PO_4 tetrahedra.

(4) The conductivity change with Na^+ content is interpreted by the structural change around Na^+.

Acknowledgement

The authors thank Professor Taichi Sato and Mr Takato Nakamura, Shizuoka University, for measuring the Raman spectra. This work was partially supported by The Okura Kazuchika Memorial Foundation and a Grant-in-Aid for Scientific Research from the Japanese Ministry of Eduction, Science and Culture.

References

1. R. S. GORDON, G. R. MILLER, T. D. HADNAGY, B. J. MCENTIRE and J. R. RASMUSSEN in "Energy and Ceramics", edited by P. Vincenzini, (Elsevier Scientific, Amsterdam, 1980) p. 925.
2. M. SLJUKIĆ, B. MATKOVIĆ and B. PRODIĆ, *Croat. Chem. Acta* **39** (1967) 145.
3. L. HAGMAN and P. KIERKEGAARD, *Acta Chem. Scand.* **22** (1968) 1822.
4. M. NAGAI, S. FUJITSU and T. KANAZAWA, *J. Amer. Ceram. Soc.* **63** (1980) 476.
5. M. PINTARD-SCREPEL, F. d'YVOIRE and F. REMY, *C.R. Acad. Soc.* **286** (1978) 381.
6. S. A. OKONENKO, S. YU. STEFANOVICH, V. B. KALININ and YU. N. VENEVTSEV, *Sov. Phys. Sol. Stat.* **20** (1978) 1647.
7. N. G. CHERNORKOV, I. A. KORSHOV and T. V. PROKOF'EVA, *Sov. Phys. Crystall.* **23** (1979) 475.
8. B. E. TAYLOR, A. D. ENGLISH and T. BERZINS, *Mater. Res. Bull.* **12** (1977) 171.
9. H. Y-P. HONG, *ibid.* **11** (1976) 173.
10. V. SHOMAKER and D. P. STEVENSON, *J. Amer. Chem. Soc.* **63** (1941) 37.
11. D. W. J. CRUICKSHANK, *J. Chem. Soc.* (1961) 5486.
12. L. PAULING, *J. Amer. Chem. Soc.* **51** (1929) 1010.
13. E. WALLEY and J. E. BERTIE, *J. Chem. Phys.* **46** (1967) 1264.
14. K. NAKAMOTO (Ed.), in "Infra-red Spectra of Inorganic and Co-ordination Compounds", (Wiley Interscience, New York, 1970) p. 113.
15. D. W. J. CRUICKSHANK and E. A. ROBINSON, *Spectrochim. Acta* **22** (1966) 555.
16. A. IMAI and M. HARATA, *Jap. J. Appl. Phys.* **11** (1972) 180.
17. W. L. ROTH, I. CHUNG and H. S. STORY, *J. Amer. Ceram. Soc.* **60** (1977) 311.
18. J. A. KAFARAS and R. J. CAVA in "Fast Ion Transport in Solids", edited by P. Vashishta, J. N. Mundy, G. Y. Shenoy, (North-Holland, Amsterdam, 1979) p.419.

Received 27 October and accepted 2 December 1980.